Postprint of the paper:
Chenyu Luan and Torgeir Moan: On Short-Term Fatigue Analysis for Wind Turbine Tower of Two Semi-Submersible Wind Turbines Including Effect of Startup and Shutdown J. Offshore Mech. Arct. Eng. Feb 2021, 143(1): 012003 (14 pages).Paper No: OMAE-19-1101 https://doi.org/10.1115/1.4047542.

ON SHORT-TERM FATIGUE ANALYSIS FOR WIND TURBINE TOWER OF TWO SEMI-SUBMERSIBLE WIND TURBINES INCLUDING EFFECT OF STARTUP AND SHUTDOWN PROCESSES

Chenyu Luan
Centre for Ships and Ocean Structures (CeSOS)
Centre for Autonomous Marine Operations and Systems (AMOS), NTNU
NO-7491 Trondheim, Norway
Chenyu.luan@ntnu.no

Torgeir Moan
CeSOS and AMOS, NTNU
NO-7491 Trondheim, Norway
Torgeir.moan@ntnu.no

ABSTRACT

Fatigue limit state design check for offshore wind turbines is based on S-N curves and the Palmgren-Miner rule approach, and focuses normally on stationary processes for which startup and/or shutdown operations induced transient load processes are normally not accounted for. However, large data bases of real-time measurements show that the shutdown and startup operations may appear in any operational conditions and the frequency of such operations could be considerable. Although design standards require fatigue design check for the transient load processes induced by startup and shutdown operations, relevant publications addressing this issue are very limited in particular for floating wind turbines.

This paper focuses on analyzing the importance of startup and shutdown induced transient load processes on fatigue damage in the tower of two MW-level horizontal axis semi-submersible wind turbines. The analysis is carried on by comparing short-term fatigue damage in several environmental conditions with and without the startup and shutdown induced transient load processes. It is found that, in many environmental conditions, startup and/or shutdown operations may make increase short-term fatigue damage by 10% to 100%; while, in some situations, the fatigue damage may be increased by up to 200%. The importance of the transient load processes on long-term fatigue damage is related to occurrence frequency of startup and shutdown events. Publicly available data indicate that the average time between two consecutive shutdown events might be less than 39 hours. However, more data and analysis are needed regarding these issues.

1. INTRODUCTION

Wind energy is an attractive source of energy in the sustainable future society (Moan et al., 2020). The wind power industry is moving from on-shore to offshore, from bottom fixed wind turbines to floating wind turbines. A representative modern floating wind turbine could be composed of a Rotor Nacelle Assembly (RNA), a tower, a hull (floater) and a mooring system. According to different features for obtaining resistance with respect to overturning moments, floating wind turbines can be classified into spar-type, tension leg platform (TLP), semi-submersible (which is also known as column stabilized) and barge wind turbines, (Butterfield et al., 2007).

Floating wind turbines operate in complex environmental conditions which result in fatigue damage (Lotsberg, 2016). Consequently, fatigue limit state design check is required by design standards for offshore wind turbines, e.g. the IEC 61400-1 design standard (IEC 2005), IEC 61400-3 design standard (IEC 2009), DNV-OS-J103 (DNV, 2013), ABS #195 (ABS, 2013) and ClassNK guideline (ClassNK, 2012), to ensure structural safety of the floating wind turbines in their design service life.

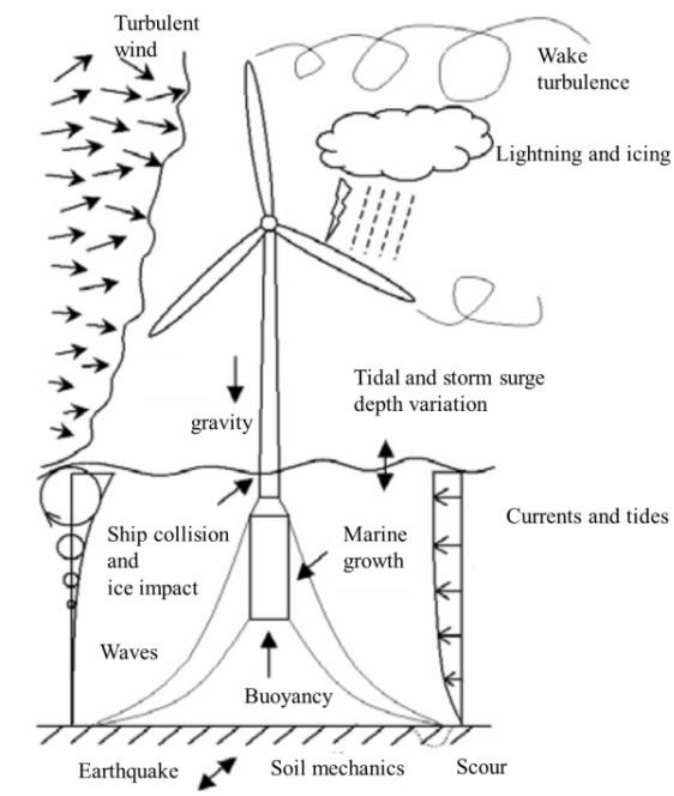

Figure 1 Environmental loads subjected on floating wind turbines (Butterfield et al., 2007)

Recommendations for design and analysis with respect to fatigue failure are available in relevant standards, e.g. DNV-RP-C203 (DNV 2010a). S-N Palmgren-Miner rule approach is normally used for fatigue assessment. For example, the approach is used by Kvittem and Moan (Kvittem and Moan, 2015) to find total fatigue damage on specified structural components of a semi-submersible wind turbine over a service life of 20 years. In conventional fatigue analysis, the fatigue damage over 20 years (D_{total}) could be calculated by using Eq. (1).

$$D_{total} = N^{20yr} \sum_{i=1}^{N^{lc}} D_i p_i \qquad (1)$$

In Eq. (1), D_i is the corresponding expected (mean) short-term fatigue damage in a T^{sim} duration stationary environmental condition i with respect to directions and statistical properties, e.g. significant wave height, mean wind speed and turbulence intensity, of incident irregular waves and turbulent winds. In practice, the expected short-term fatigue damage is obtained by taking the averaged value of the corresponding short-term fatigue damage simulated by a set, e.g. about 10, of different random seeds. The expected values are used to reduce stochastic uncertainties in the simulated short-term fatigue damage. p_i is probability of the environmental condition i obtained from a corresponding joint distribution for wind and waves. Note that $\sum_{i=1}^{N^{lc}} p_i = 1$. N^{lc} is total number of the environmental conditions. $N^{20yr}$is total number of stationary environmental conditions in 20 years.

In the conventional approach shown by Eq. (1), fatigue damage over a given period, e.g. 20 years, is considered as a summation of the short-term fatigue damage of each stationary environmental condition multiplying by the number of occurrence of the environmental condition during the given period. In each short-term analysis, the analyzed floating wind turbine oscillates around its corresponding mean position. The mean position is determined by mean component of environmental loads, e.g. aerodynamic loads and mean wave drift forces.

Consequently, the conventional approach fails to represent the feature that, in reality, environmental condition varies continuously, and account for fatigue damage of transient load processes during startup and shutdown operations.

For short-term fatigue damage analysis for semi-submersible wind turbines, fatigue damage of the transient load processes might be considerable and make the short-term fatigue significantly increase in comparison to the corresponding short-term fatigue damage for which the transient load processes are not accounted for. This is because large change in mean horizontal offset and tilt angle might be involved in the transient load processes and result in cycles with relatively large stress ranges. In contrast to bottom fixed wind turbines, mean component of aerodynamic loads on semi-submersible wind turbines could result in relatively much larger mean

horizontal offset and tilt angle. In addition, fatigue damage of the transient load processes is related to control method and parameters of the servo system for startup and shutdown operations.

The influence of the transient start-up and shut-down load processes on the long-term fatigue damage depends on the frequency of these transient events in the long-term period.

According to requirements specified in DNVGL (2012) and classifications used by Valerie et al (2012), shutdown events can be classified as Groups A, B, and C. Definitions of the groups and occurrence frequencies of the shutdown events, which are obtained from analysis for 327,000 turbine-days real-time data collected from more than 800 land based 1.3 to 1.4 MW horizontal axis wind turbines, are given in Table 1. From Table 1, it could be known that the shutdown events in Groups A and B may appear in any operational conditions and number of the shutdown events may be considerable, while an automatic startup may occur following a shutdown events in Group B.

Analysis with respect to fatigue damage induced by startup and shutdown operations is required by standards for offshore wind turbines. However, as far as the authors know, publications for offshore wind turbine fatigue analysis including the transient load processes are very limited, in particular for floating wind turbines. Hence, the importance of the transient load processes on the fatigue damage has not been sufficiently clarified.

This paper focuses on shedding light on the importance of the startup and shutdown induced transient load processes on fatigue damage on tower of two semi-submersible wind turbines by comparing short-term fatigue damage in representative environmental conditions with and without the transient load processes induced by startup and shutdown of the wind turbines. The importance of the transient load processes on long-term fatigue damage is discussed as well.

The specification of the two semi-submersible wind turbines and environmental conditions, as well as the relevant methodology for time-domain simulation and analysis, results and discussions are given in following.

Table 1 Definitions of the groups and occurrence frequencies of the shutdown events

Shutdown Events	Definition (according to DNVGL 2012 and Valerie et al 2012)	Occurrence frequency of shutdown event (Based on data of MW level land-based wind turbines)	Notes
Group A	Shutdown events to take the turbine out of service due to fault state or maintenance operations	In average, one shutdown event per 39 hours per turbine (Valerie et al 2013)	
Group B	Shutdown events initiated by the control system of the wind turbine as measurements exceed alarm limiting values specified by operators but are below the limiting values for activating the safety system of the wind turbine.	The system of offshore wind turbines is complex involving many measurements for control and monitoring purposes and operator specified limiting values. Therefore, the probability for the measurements exceeding the alarm limiting values may be higher than the probability of fault states. Durations of shutdown-automatic startup (see explanations in the right hand side column) are expected to be short, e.g. in 10 mins, and are included in "Reserve Shutdown-Other" events, see (Valerie et al 2012), who mentioned that a large number of very short "Reserve Shutdown-Other" events were observed in the analyzed data.	For cases defined in Section 2.3.2 (DNVGL 2012), the offshore wind turbine is permitted to start again automatically without clearance following a turbine shutdown. The automatic startup is limited to a few times, e.g. 3 times, every 24 hours for exceedance of most of the limiting values and counts for automatic startup times corresponding to different limiting values can be undertaken separately.
Group C	Shutdown events operated by the control system of the wind turbine as the state is not appropriate for power generation, e.g. wind speed exceeds the cut-out wind speed, while there is no fault state.		

2. DEFINITION OF THE 5-MW-CSC AND OC4 SEMI-SUBMERSIBLE WIND TURBINES

The two semi-submersible wind turbines are named 5-MW-CSC and OC4 Semi, respectively. The configuration of the 5-MW-CSC in an earth fixed global coordinate system (x^g-y^g-z^g) is shown in Figure 2. When the 5-MW-CSC is located in calm water, the origin of the global coordinate system (O^g) is located at the geometrical center of the water plane area. The configuration of the OC4 Semi is shown in Figure 3.

Each semi-submersible wind turbine is composed of a rotor nacelle assembly (RNA), tower, hull and three catenary mooring lines. Each semi-submersible hull is composed of three side columns and a central column. The tower is mounted on the central column. For the 5-MW-CSC, the columns are connected by three pontoons as an integrated structure, while for the OC4 Semi, the columns are connected by braces.

The RNA and tower of the 5-MW-CSC is identical to the one of the OC4 Semi. Properties of the RNA are described by Jonkman et al (2009), and the control system and tower are described in (Jonkman 2010). The overall dimensions of the hulls and design of the mooring lines of the 5-MW-CSC and OC4 Semi are described in (Luan et al., 2016) (Robertson et al., 2012).

Linearized roll and pitch restoring stiffness (Faltinsen, 1990) of the OC4 Semi in calm water are approximately twice of the corresponding stiffness of the 5-MW-CSC. Mean tilt angles of the 5-MW-CSC and OC4 Semi in the operational condition in rated wind speed are around 6 and 3 degrees, respectively. The volume of displaced water of the 5-MW-CSC and OC4 Semi are 10,298 $m^3$and 13,917 m^3, respectively. The natural periods of 6 d.o.f.s rigid-body motions of the semi-submersibles are obtained by using the numerical models described in Section 4.1 to carry out decay tests and are given in Table 2.

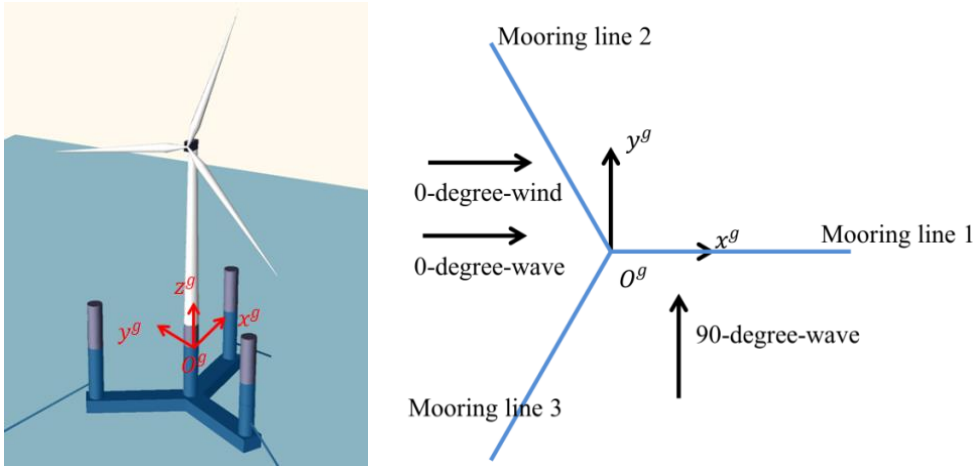

Figure 2 Configuration of the 5-MW-CSC (Luan et al., 2016)

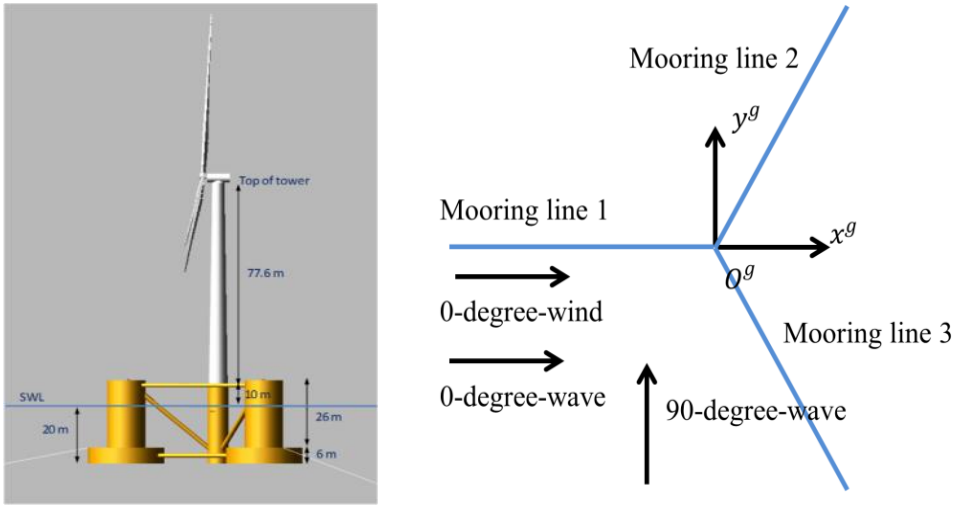

Figure 3 Configuration of the OC4 Semi (Robertson et al., 2012)

Table 2 Natural periods of 6 d.o.f.s rigid-body motions of the 5-MW-CSC and OC4 Semi

Natural periods [s]	Surge	Sway	Heave	Roll	Pitch	Yaw
5-MW-CSC	78.5	78.5	25.8	32.4	32.4	58.2
OC4-Semi	114.8	114.8	17.2	26.0	25.8	80.0

3. ENVIRONMENTAL CONDITIONS

Table 3 Environmental conditions.

Case Name	Mean wind speed at nacelle [m/s]	Turbulence Intensity [%]	Hs [m]	Tp [s]	Wave/wind directions [degree]	Occurrence probability of corresponding mean wind speed.	Note
F100	6.8	23	1.0	5.5	0/0	0.2062 (the probability of mean wind speed no more than 6.8 m/s)	Operational condition (Occurrence probability for short-term environmental conditions for which mean wind speed is no more than 23.4 m/s is 99.59%
F110				7.8			
F120				10.1			
F200	8.0	17	2.0	6.0		0.304 (the probability of mean wind speed in between of 6.8 m/s and 8 m/s)	
F210				8.5			
F220				11.1			
F300	11.0	15	3.0	6.6		0.2207 (the probability of mean wind speed in between of 8.0 m/s and 11.0 m/s)	
F310				9.4			
F320				12.2			
F400	13.8	14	4.0	7.1		0.1313 (the probability of mean wind speed in between of 11.0 m/s and 13.8 m/s)	
F410				10.2			
F420				13.3			
F500	16.5	13	5.0	7.5		0.0751 (the probability of mean wind speed in between of 13.8 m/s and 16.5 m/s)	
F510				10.7			
F600	18.9	12.6	6.0	7.8		0.0353 (the probability of mean wind speed in between of 16.5 m/s and 18.9 m/s)	
F610				11.1			
F700	21.3	12	7.0	8.1		0.0163 (the probability of mean wind speed in between of 18.9 m/s and 21.3 m/s)	
F710				11.5			
F720				15			
F800	23.4	11.9	8.0	8.5		0.007 (the probability of mean wind speed in between of 21.3 m/s and 23.4 m/s)	
F810				12.1			
F820				15.7			

This paper focuses on short-term analysis in operational conditions of the semi-submersible wind turbines. Twenty-two environmental conditions are selected from joint distribution for wind and waves at a site in the northern North Sea (Li, et al. 2015). The environmental conditions are tabulated in Table 3.

Irregular waves and turbulent winds at the site could be described by two-parameter (i.e. Hs and Tp) JONSWAP spectrums, and Kaimal wind spectrums and normal turbulent wind model, respectively. The significant wave height (Hs) of the selected conditions varies from 1 m to 8 m, while mean wind speed increases with increase of the significant wave height, from 4.9 m/s to 23.4 m/s. Note that the cut-in, rated and cut-out wind speeds are 3 m/s, 11.4 m/s and 25 m/s, respectively. The turbulent intensity factors of the winds are determined by the mean wind speed by using the formula for wind class C (low turbulent wind) given in IEC (2009), since offshore wind is less turbulent than onshore wind.

For a given mean wind speed shown in Table 3, the corresponding significant wave height and Tp of FX10 (X corresponds tp the mean wind and speed and could be 1, 2, 3, 4, 5, 6, 7,or 8) are expected values of the environmental conditions which correspond to the mean wind speed. Dynamic responses of floating wind turbines could be sensitive to values of Tp (the peak period of JONSWAP spectrum). Therefore, for each selected Hs, two or three values of Tp are selected. Directions of incident wind and waves are shown in Figure 2.

4. METHODOLOGY

Time-domain numerical models are used to simulate short-term responses of the 5-MW-CSC and OC4 Semi in the environmental conditions specified in Section 3 with and without transient load processes (startup and shutdown). Axial forces in sectional forces and moments in tower base and tower top of the semi-submersible wind turbines are simulated and used to derive realizations of corresponding nominal stresses. The realizations of the nominal stresses, rainflow counting algorithm and S-N Palmgren-Miner rule approach is used to assess corresponding short-term fatigue damage rates.

4.1 Time-domain numerical model for global response analysis

Numerical models used in this paper are developed in Simo/Riflex/Aerodyn which is a state-of-the-art time-domain code for simulation of global responses of floating wind turbines, see (Ormber et al., 2011) (Ormber and Bachynski, 2012) (Luxcey et al., 2011) (Moriarty and Hansen, 2005), and has been used by some researchers, e.g. see (Nejad et al., 2015) (Moan, 2015) , (Bachynski et al., 2013) and (Bachynski et al., 2014).

Flow chart of the numerical models is given in Figure 4. For each semi-submersible wind turbine, the hull is considered as a rigid-body with 6 d.o.f.s and modelled by six motion equations in Simo (MARINTEK, 2011). The blades, shaft of the drive train inside the nacelle, tower and mooring lines are modeled as beam elements in Riflex (MARINTEK, 2013). Motions of lower end node of the tower and upper nodes of the mooring lines rigidly follow the motions of the hull. The hub and nacelle are modeled as rigid mass points attached on the shaft and top of the tower. The shaft is rotational about its longitudinal axis. The rotational d.o.f. is achieved by applying a flex joint (MARINTEK, 2013) on the beam element of the shaft. The blades are connected to the tower through the shaft. Loads on the blades, hub, shaft and generator torque are transferred through the flex joint to the beam element of the tower.

Aerodynamic loads on the blades and tower are calculated in Aerodyn (Moriarty and Hansen, 2005); while wind fields are generated by Turbsim (Jonkman 2009) using 32×32 points in the rotor plane with time step of 0.05 s and specifications of the environmental conditions described in Section 3.

Aerodyn and a Java controller are coupled to Riflex through a dll file (Ormber and Bachynski, 2012). The Java controller is used to model the startup and shutdown process (Bachynski et al., 2013), effect of pitch control on aerodynamic loads on the three blades and effect of the generator inside the nacelle on the power production and generator torque which is simulated based on rotational speed of the shaft. The Java controller is based on the NREL-developed controller described by Jonkman (2010).

Hydrodynamic loads on the mooring lines are accounted for by the Morison formula, while first order potential flow theory and drag term of the Morison formula are used to account for hydrodynamic loads on the semi-submersible hulls (Luan et al 2017).

Non-dimensional drag (C_d) and mass (C_a) coefficients used in the Morison formula selected by using DNV standard (DNV, 2010b) and are given in Table 4. The pontoons of the 5-MW-CSC have box-shape cross-sections. Upper and lower edges of the box-shape cross-section represent width of the pontoons, while side edges represent height of the pontoons. Coefficients corresponding to the width and height of the pontoons are given respectively. Regarding coefficients for the OC4 Semi, as shown in Figure 3, the hull of the OC4 Semi is composed of three side columns, a central column and braces in between of the columns. Each side column of the OC4 is divided into two parts, named “upper column” and “base column”, with 12 m and 24 m column diameters, respectively. First order potential flow theory is used to account for hydrodynamic loads on the central and side columns of the OC4 Semi. However, Morison formula is used to model hydrodynamic loads on the braces since the braces are slender structures comparing to wave length of the incident waves.

Numerical solutions of the Simo/Riflex/Aerodyn models are obtained by using the Newmark-β numerical integration ($\beta = 3.9$ and $\gamma = 0.505$). The time step is set to be 0.005 seconds. Rayleigh damping, which is a linear combination of the Riflex generated global mass and stiffness matrices, is used for modelling effect of structural damping. The corresponding mass and stiffness proportional coefficients are set to be 0 and 0.005, respectively. More explanations are given in (MARINTEK, 2013).

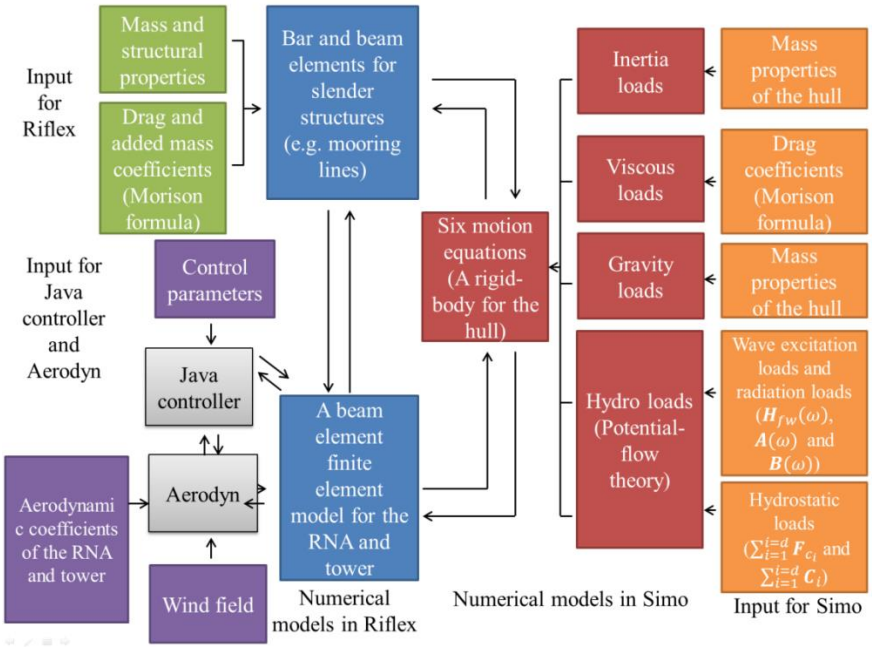

Figure 4 Flow chart of a time-domain numerical model of a generic horizontal axis floating wind turbine developed in Simo/Riflex/Aerodyn (the conventional approach) (Luan et al., 2017)

Table 4 Non-dimensional Morison coefficients used for modelling hydrodynamic loads. PF means that the hydrodynamic loads are modelled by the conventional hybrid frequency-time domain approach which is based on potential flow theory, see (Luan et al. 2017).

Semi-submersible hulls	Structural component	C_d	C_a
5-MW-CSC	Central column	0.5	PF
	Side columns	0.5	
	Pontoons (width)	2.1	
	Pontoons (height)	1.7	
	Mooring lines	1.2	1
OC4 Semi	Braces	0.63	0.63
	Central column	0.61	PF
	Upper columns	0.56	
	Base columns	0.68	
	Base column (longitudinal direction)	4.8	
	Mooring lines	1.1	1

4.2 Short-term fatigue damage analysis

Realizations of sectional forces and moments in tower base and tower top of the 5-MW-CSC and OC4-Semi in the selected short-term environmental conditions are simulated by using the numerical model described in Section 4.1 and used to derive nominal stresses.

Nominal axial (σ_x) and shear (τ) stresses at 8 points, see Figure 5, on tower base and tower top are calculated by using Eq.s 2 and 3. The outer radius of the thin-walled circular cross-section at tower base is r. In the cross-section at tower base, x^b-y^b-z^b is a body-fixed coordinate system with origin O^b located at geometrical center of the tower base. Positive directions of the x^b-y^b-z^b coordinate system are identical to positive directions of the x^g-y^g-z^g coordinate system. The positive direction of z^b axis is pointed from geometrical center of the tower base to geometrical center of the tower top. Internal loads in the cross-section are denoted as $\boldsymbol{F} = [F_1, F_2, F_3, F_4, F_5, F_6]$ in the corresponding x^b-y^b-z^b coordinate system and acting on O^b. Positive value of $\sigma_x(t,\theta)$ means the corresponding point is in tension. Positive direction of $\tau(t,\theta)$ is defined as anti-clockwise. In Eq.s (2 and 3), A is the cross-sectional area, J is polar moment of area, I_{x^b} and I_{y^b} are second moment of area for the cross-section about x^b and y^b axes, respectively. Note that θ for Point 1 is 0-degree.

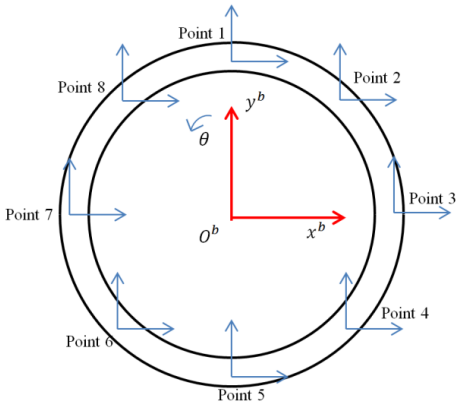

Figure 5 Points on thin-walled circular cross-section at tower base with outer radius r

$$\sigma_x(t,\theta) = \frac{F_3}{A} + \frac{F_4}{I_{x^b}} r\cos(\theta) + \frac{F_5}{I_{y^b}} r\sin(\theta) \qquad (2)$$

$$\tau(t,\theta) = \frac{F_6 r}{J} - \frac{2F_1}{A}\cos(\theta) - \frac{2F_2}{A}\sin(\theta) \qquad (3)$$

For each stress realization, rainflow counting algorithm, which is implemented in WAFO (Brodtkorb et al., 2000), is used to deal with peaks and valleys of the realization to identify equivalent cycles with corresponding stress ranges.

We denote total number of identified cycles of a stress realization as N_0. Stress range of number i cycle is denoted as $\Delta\sigma_i$. According to Palmgren-Miner rule, fatigue damage rate (D) induced by the stress realization is calculated by Eq. (4).

$$\mathrm{D} = \sum_{i=1}^{N_0} \frac{1}{N_i} \qquad (4)$$

N_i corresponds to $\Delta\sigma_i$ and can be obtained from the relevant SN curves given in (DNV 2010a). For transverse butt welds between tower base and central column of semi-submersible hulls, we have:

$$\log N_i = log\bar{a} - mlog\left(\Delta\sigma_i \left(\frac{t_{sc}}{t_{ref}}\right)^k\right) \qquad (5)$$

where, m is negative inverse slope of the SN curve (fatigue exponent), $log\bar{a}$ is intercept of $\log N_i$ axis, t_{ref} is the reference thickness, which is equal to 25 mm, for welded connections other than tubular joints. t_{sc} is the thickness for weld connections.

The thickness of the tower base and tower top are 0.0268m and 0.0192 m respectively. Parameters for the selected SN curves for tower top and tower base fatigue damage calculation are given in Table 5, based on SN curves in air tabulated in Table 2-1 in (DNV 2010a).

Table 5 Selected two slope SN curves for short-term fatigue damage rate calculated at tower base and tower top

SN curves	$N_i \le 10^7$ cycles		$N_i > 10^7$ cycles		Stress range at 10^7 cycles	Thickness exponent k
	m_1	$log\bar{a}_1$	m_2	$log\bar{a}_2$		
C1	3	12.449	5	16.081	65.50	0.15
D	3	12.164	5	15.606	52.63	0.20
F	3	11.855	5	15.091	41.52	0.25

5. RESULTS AND DISCUSSIONS

5.1 Short-term response analysis and startup and shutdown operations induced transient load processes

In each short-term analysis for each semi-submersible wind turbine in each selected environmental condition, 5,600 seconds responses are simulated. As an example, pitch motion of the 5-MW-CSC in an operational condition with and without the transient load processes induced by startup and shutdown operations is shown in Figure 6.

For the black solid line in Figure 6, the wind turbine starts at the beginning of the simulation ($t = 0$ s) with a constant wind speed and corresponding irregular waves, and is subjected to turbulent winds from $t = 1{,}000$ s to the end of the simulation. The constant wind speed is equal to mean speed of the turbulent winds at hub of the turbine. At $t = 1{,}000$ s, transient load process, which is induced by the startup at $t = 0$, has been damped to a negligible level. Therefore, from $t = 1{,}000$ s to $t = 5{,}600$ s, the 4,600

seconds realization represented by the black solid line is considered as a stationary realization which does not include transient load process induced by initiation of startup and shutdown operations.

For the red dashed line and blue solid line in Figure 6, the wind turbines start at $t = 1{,}000$ s in the same turbulent winds as the model represented by the black solid line and are shut down at $t = 4{,}600$ s. Therefore, from $t = 1{,}000$ s to $t = 5{,}600$ s, the 4,600 seconds realizations represented by the red dashed line and blue solid line are considered as realizations with transient load processes induced by startup and shutdown operations.

Note that, in each simulation, the 5-MW-CSC is subjected to irregular waves from the beginning to the end while fatigue damage is calculated on base of corresponding stress realizations from $t = 1{,}000$ s to $t = 5{,}600$ s.

Pitch angles of the blades of the turbine are manipulated to generate torque against rotation of the rotor to shut down the turbine. During a shutdown operation, the pitch angle of the turbine blades could be rotated by different speed from the instantaneous position of each blade to the target position of the blades specified by the control system. In this paper, the effect of two different blade pitch angle rotational speeds, i.e. 2 degree/s and 8 degree/s, are analyzed since aerodynamic loads on the blades are affected by the speeds. The red dashed line and solid blue line represent models with the 2 degree/second and 8 degree/second, respectively. Consequently, the red dashed line and blue solid line are identical except for realizations after the initiating of the shutdown at $t = 4{,}600$ s. More detailed analysis for the difference between the red dashed line and blue solid line are given in later part of the present paper.

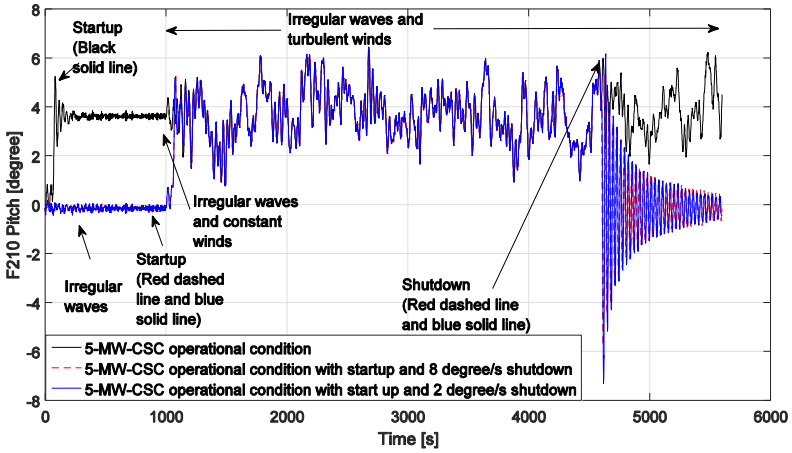

Figure 6 Simulated pitch motions of 5-MW-CSC in F210 with and without startup and shutdown

5.2 Comparison of short-term fatigue damage at different positions of the tower base and tower top

We find that fatigue damage of the tower base and tower top is dominated by variations of nominal stresses at the point 3 and point 7 in the cross-sections of the tower base and tower top induced by variations of corresponding fore-aft bending moments. The influence of shear stresses is found to be negligible, see Figure 7.

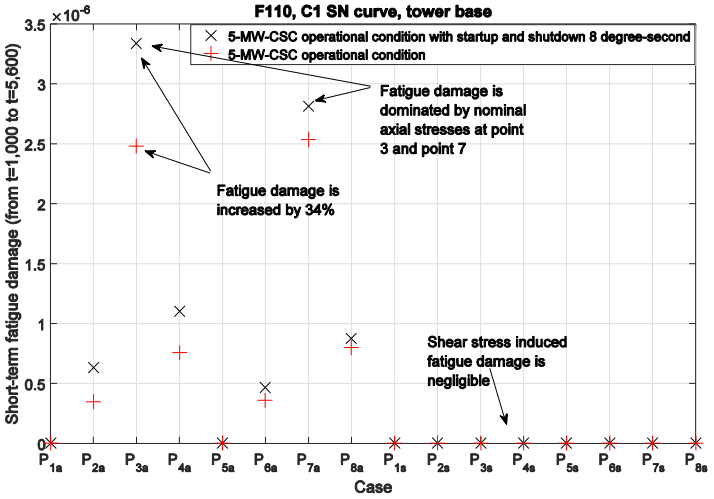

Figure 7 Short-term fatigue damage rates for the points on tower base in F110 with C1 SN curve. P_{ia} represents axial stress of point i. P_{is} represents shear stress of point i.

5.3 Fatigue damage of the transient load processes and method for mitigating the damage

The transient load processes induced by startup and shutdown may result in cycles with relatively large stress ranges compared to the cycles induced by wind and wave loads in the stationary operational condition. Fatigue damage of the transient load processes and method for mitigating the damage are discussed in the following.

5.3.1 Shutdown operation

As a representative example, realizations of nominal stress at Point 3 of the tower base of the two models in F210, see Table 3, with and without shutdown operation induced transient processes are shown in Figure 8. As shown by the figure, shutdown operation could result in several cycles with large stress range.

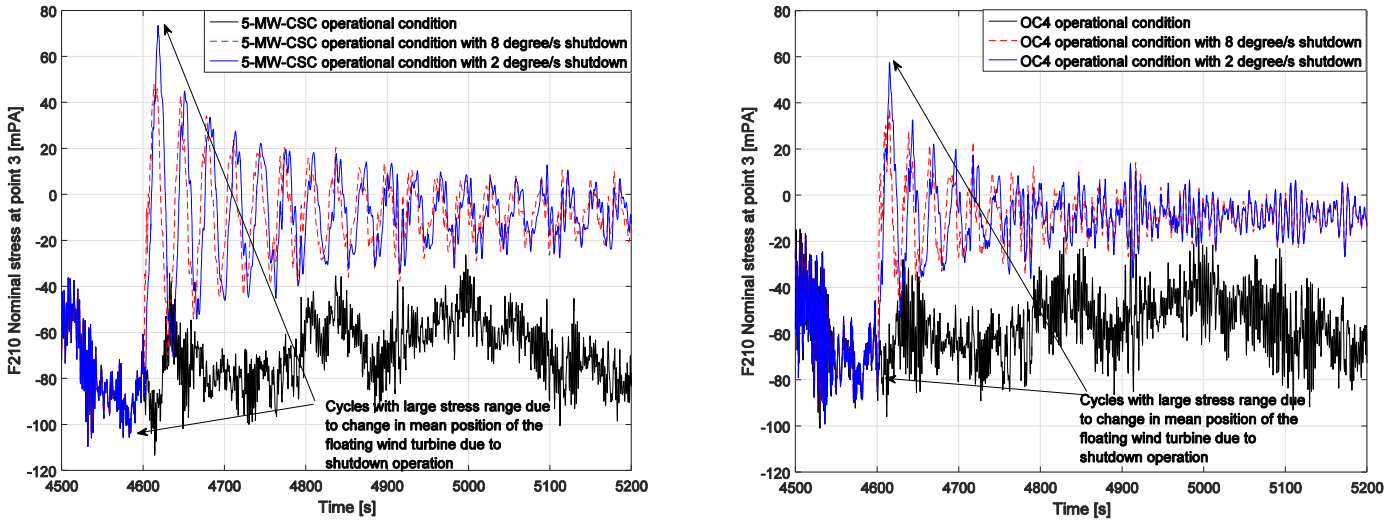

Figure 8 Realizations of nominal stress at point 3 of the tower base of 5-MW-CSC (the left figure) and OC4 (the right figure) in F210 with and without shutdown (Zoom-in)

Comparisons of fatigue damage of cycles identified from the transient processes induced by shutdown operations and corresponding stationary responses are shown in Figure 9. Note that the transient processes and stationary responses are referred to the parts of the corresponding realizations of nominal stress at Point 3 of the tower base, from $t = 4{,}600$ s to $t = 5{,}600$ s.

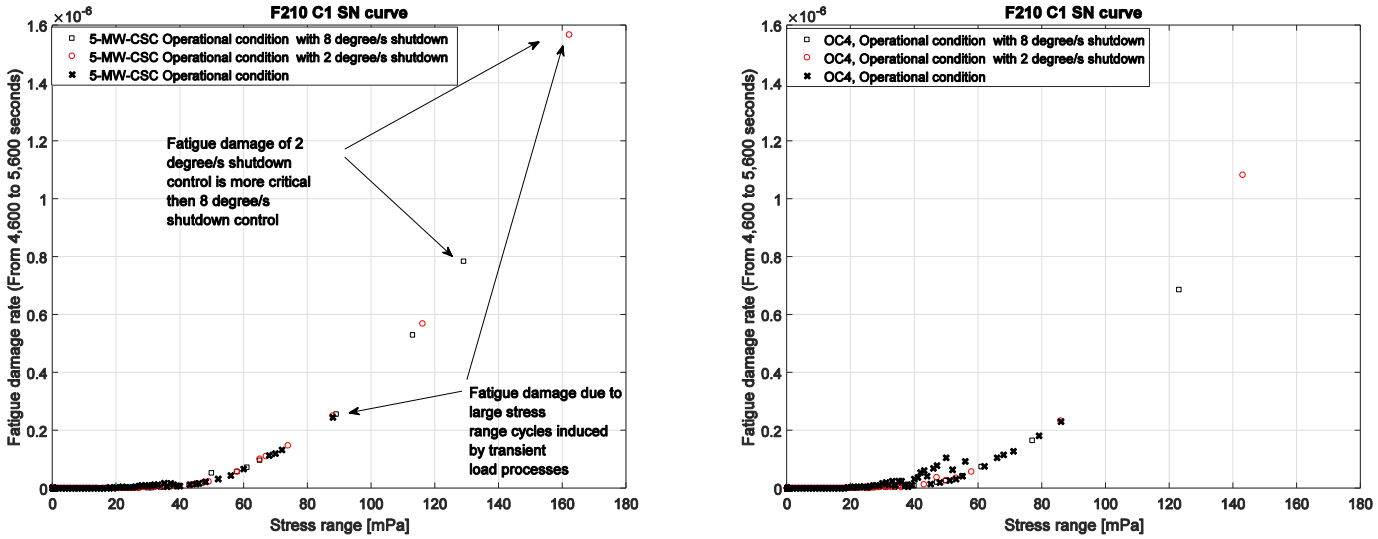

Figure 9 Cycles with different stress ranges and corresponding fatigue damage, F210 (see Table 4), from 4,600 s to 5,600 s, C1 SN curve, nominal stress at point 3 of tower base. Note that a point on (x,y) in the figure means fatigue damage rate due to cycles with stress ranges in (x-1,x] is y. x is an integer.

The comparisons show that fatigue damage of the cycles with large stress range identified from the transient processes could be much larger than fatigue damage of cycles under stationary conditions in F210. The importance of the fatigue damage of the transient processes on short-term fatigue damage is further analyzed in Section 5.4.

Variation of the nominal stress at Point 3 on the tower base is dominated by variation of fore-aft bending moment in the tower base. Simply speaking, for each model, the bending moment in the tower base is determined by aerodynamic loads, inertial loads and gravity force on the part of the structure above tower base. The inertial loads and gravity force are related to the motions of the structure. The aerodynamic loads are related to the procedure of the shutdown operation. Consequently, for each model, stress ranges of the cycles of the transient processes are related to the mean tilt angle, hydrodynamic viscous damping and procedure of shutdown operation.

For semi-submersible wind turbines, the mean tilt angle and hydrodynamic viscous damping are related to the structural design of semi-submersible hulls. The mean tilt angles of the 5-MW-CSC and OC4 Semi in operational condition in rated wind speed are around 6 and 3 degrees, respectively; while, cycles with larger stress range are identified from the transient load processes of the 5-MW-CSC than the corresponding one of OC4 Semi, see Figure 9.

For each model, two shutdown operation procedures are analyzed. The two procedures are that pitch angle of the turbine blades are rotated to feather (Jiang et al 2013) at 2 degree/s and 8 degree/s, respectively. As shown as an example in Figure 9, in general, fatigue damage of the transient load processes induced by shutdown operation with 8 degrees/s control is less than that with a 2 degrees/s control.

The reason is as follows:

Realizations of the nominal stress at Point 3 of the tower base and pitch motion (from $t = 4{,}600$ s to $t = 4{,}640$ s) of 5-MW-CSC are shown in Figure 10. The figure shows that, after initiation of shutdown operation, the first peaks of the stress realizations for 8 degrees/s control and 2 degrees/s control, which result in cycles with large stress range, are at t=4,615s and t=4,618 s respectively and, approximately, in accordance to the first peaks of the corresponding pitch motion realizations.

Meanwhile, the corresponding realizations of the thrust force on the rotor, which is a resultant of aerodynamic loads on the blades, are shown in Figure 11. The figure shows that, after initiation of shutdown operation for each model, the magnitude of the thrust force will decrease to a negative value. The negative value means that the rotor is actually subjected by a pull force, which is in opposite direction of the thrust force. When the pull force reaches its peak value, the magnitude of the force will decrease to a negligible level.

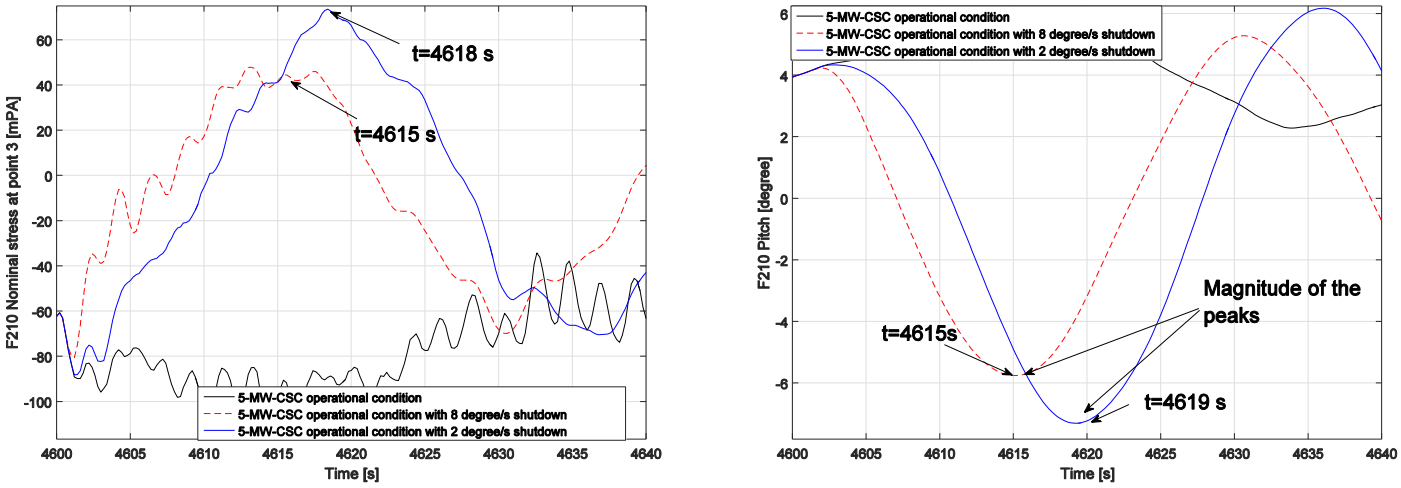

(a) Nominal stress at point 3 of the tower base

(b) Pitch motion

Figure 10 Realizations of nominal stress at point 3 of the tower base of 5-MW-CSC (the left figure) and pitch motion of 5-MW-CSC (the right figure) in F210, see Table 4, (from $t = 4,600$ s to $t = 4,640$ s)

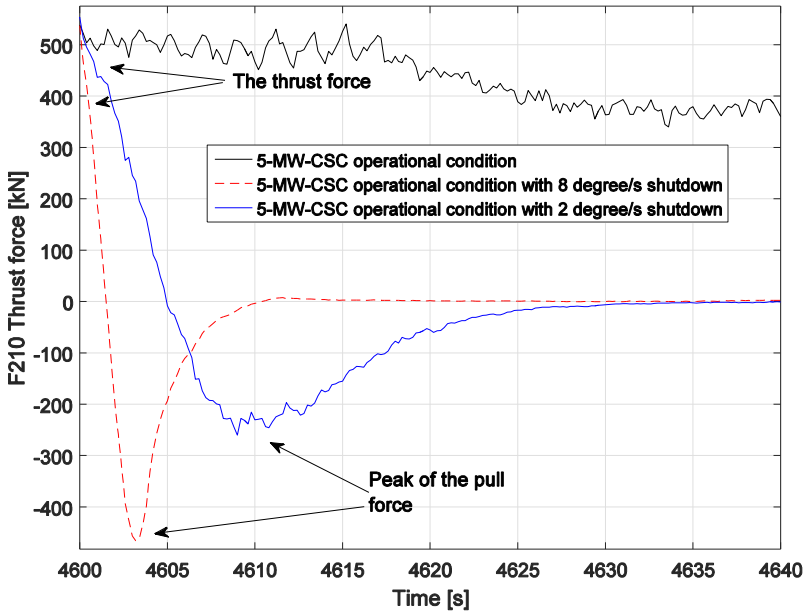

Figure 11 Realizations of the thrust force of 5-MW-CSC in F210 (from $t = 4,600$ s to $t = 4,640$ s)

As shown in Figure 11, by slowing down the blade pitch rotational speed for shutdown operation from 8 degree/s to 2 degree/s, the peak magnitude of the pull force on the rotor is reduced; while the duration, for which the magnitude of the force on the rotor is decreased to a negligible level, is increased from approximately 10s to 30s. However, the reduction of the blade pitch rotational speed results in larger pitch motion and cycles with larger stress range as shown in Figure 10.

The magnitude of the pitch motion is related to hydrodynamic and aerodynamic load effects which are coupled with the blade pitch angle control and dynamic motions of the model. Generally speaking, the simulated pitch motion indicates that, in the duration from initiation of shutdown to $t = 4{,}619$ s, the model with 2 degree/s control is subjected to less damping load effect and/or gets more kinematic energy from external loads than the model with 8 degree/s. A parametric study with respect to pitch rotational speeds could be carried out in future to find an optimal operational procedure for shutdown and/or shed more light on mechanical effect of blade pitch angle control on dynamic responses of floating wind turbines.

The simulated results shown in Figures 10 and 11 imply that the extreme aerodynamic load on floating wind turbine rotors during shutdown operation might be reduced by slowing down pitch rotational speed of the blades; however on the other hand the wind turbine structures will be subjected to more fatigue damage. Consequently, the importance of fatigue damage of the transient load processes on short-term and long-term fatigue damage is analyzed in Sections 5.4 and 5.5, respectively.

5.3.2 Startup operation

Publicly accessible information about startup control of floating wind turbines is very limited. The simulated dynamic responses of the 5-MW-CSC and OC4 Semi show that the NREL-developed controller described by Jonkman (2010) can appropriately startup the models in environmental conditions for which mean wind speed is below or around rated wind speed. However it is challenging to startup floating wind turbines in the above rated wind condition. The reason is that the NREL-developed controller will not adjust blade pitch angles to reduce aerodynamic loads on the rotor until rotation of the rotor first reaches its rated rotational speed. To solve this limitation, we suggest that blade pitch angles could be rotated to a specified angle, which is in accordance to mean wind speed, in the duration from initiation of startup to the time at which the rotor first reaches its rated rotational speed. To illustrate the effect of this approach a representative example with startup of the 5-MW-CSC in F720 is shown in Figures 12 and 13. Note that the startup transient load process is not sensitive to rotational speed of blade pitch since the simulation results of 8 degrees/s and 2 degrees/s blade pitch angle control are almost identical.

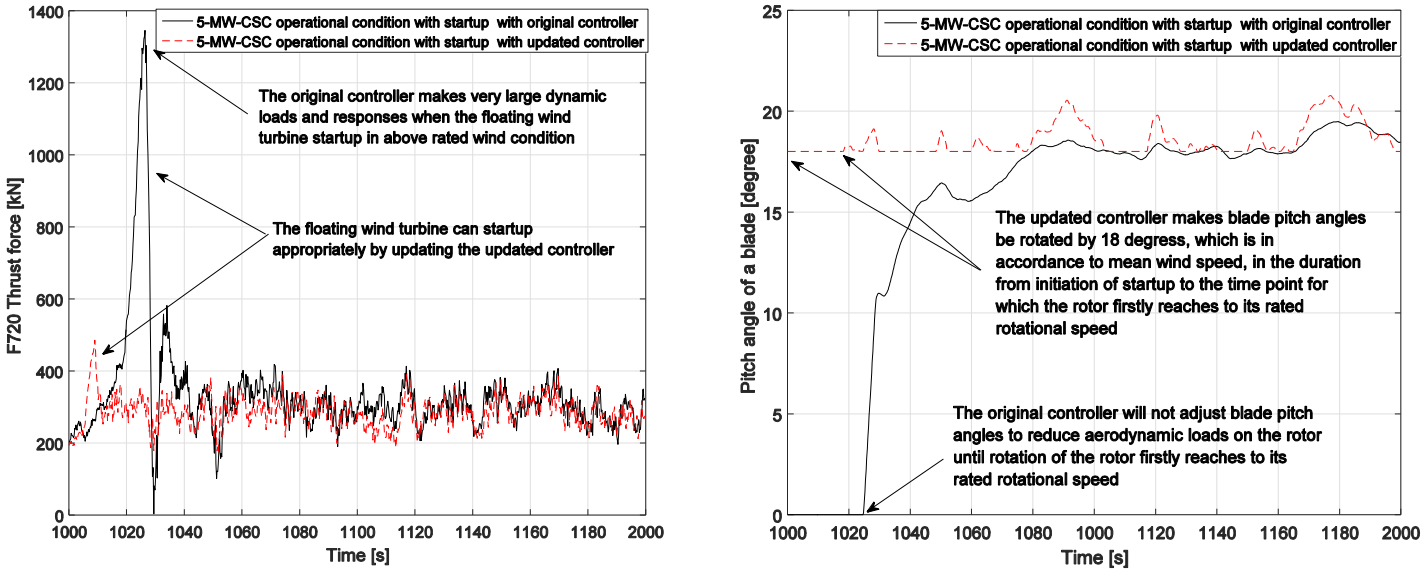

Figure 12 Realizations of the thrust force on the rotor (left) and pitch angle of a blade of 5-MW-CSC in F720 with the (original) NREL controller and the updated controller during startup. Startup operation is initiated at t=1,000 s.

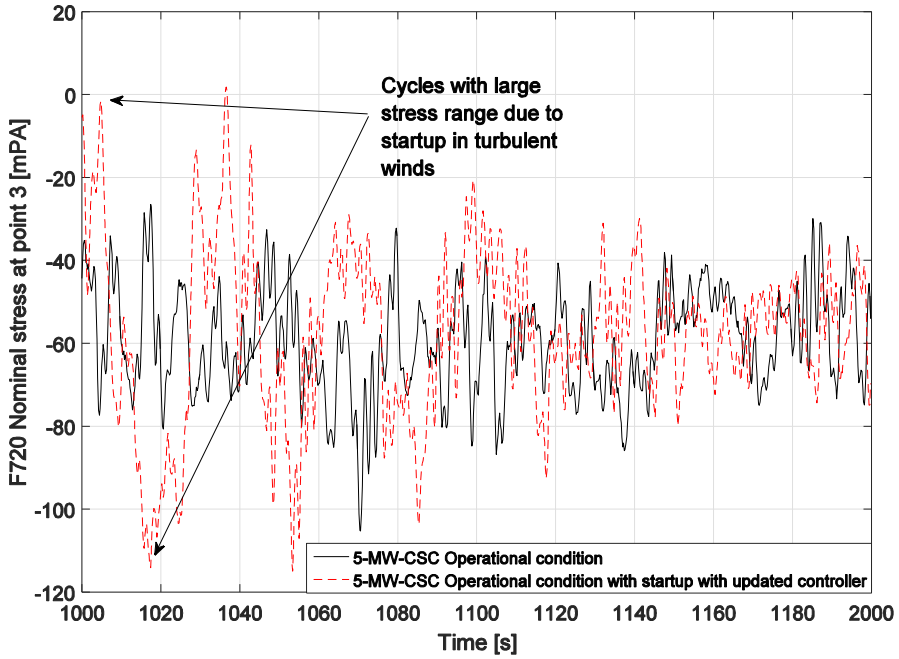

Figure 13 Realizations of the nominal stress at point 3 of the tower base and pitch angle of a blade of 5-MW-CSC in F720 with and without startup operation, based on the updated NREL controller. Startup operation is initiated at t=1,000 s.

In general, cycles with relatively large stress ranges are observed in startup operations of the models in above rated wind conditions, see Figure 13 as an example. It could be expected that fatigue damage of the startup operation may be reduced by developing and implementing an even more advanced control system which make the blade pitch angles be more appropriately controlled in accordance to rotational speed of the rotor and generated power to avoid large aerodynamic loads on the rotor and to mitigate the increase of kinetic and potential energy of the models during the startup operations. However, the disadvantages of increased complexity and reduced reliability of the control system should also be considered. More information from industry is needed.

The importance of fatigue damage during the startup operation based on the updated NREL controller is analyzed in Sections 5.4 and 5.5.

5.4 Importance of the transient load processes on short-term fatigue damage

Short-term fatigue damage with and without the startup and shutdown operation is analyzed. Each short-term fatigue damage is calculated based on the corresponding 4,600 seconds realization as shown in Section 5.1. Note that, for each environmental condition, the 5-MW-CSC and OC4 semi-semi with and without the transient load processes are subjected to the same wind and waves. This makes the models be comparable.

Some calculated fatigue damage rates are given in Table 6. For example, if the fatigue damage rate is calculated by using SN curve C1, the transient load process increases the short-term fatigue damage rate of the point 3 of the tower base of the 5-MW-CSC and OC4-Semi in F310 by 23% and 9%, respectively; while the relative difference for the OC4 Semi with respect to some cases, e.g. F110 and F210, could even be a negative value. The negative values mean that the fatigue damage induced by a shutdown operation could result in smaller fatigue damage than for the corresponding stationary condition. This is because, although shutdown operation may result in several cycles with large stress ranges after initiation of the shutdown, in the other part of the transient process, fatigue damage on the floating wind turbine is reduced due to significant reduction of the aerodynamic loads on the RNA and tower. Aerodynamic loads on parked floating wind turbines in the below rated wind speeds are negligible compared to the corresponding aerodynamic loads on floating wind turbines in the operational condition; while in this paper, a shutdown process is defined from the initiation of shutdown ($t = 4{,}600$) to the end of numerical simulation ($t = 5{,}600$).

For the 5-MW-CSC, we observe that the transient load processes due to shutdown operation can result in a considerable increase of short-term fatigue damage for the tower base and tower top for the cases F100 to F320. In these cases, as shown in Table 3, irregular waves are moderate (Hs is no more than 3 meters); while the turbine operates in below rated speed or rated wind speed. Note that the occurrence probability of environmental conditions, for which mean wind speed is no more than rated wind speed, is 73.09%. While, Table 1 shows that impact of the fatigue damage due to the transient load processes on short-term fatigue damage of above mean wind speed environmental conditions is limited; however, it should be emphasized that, as shown in Section 5.3, fatigue damage of the transient processes is very sensitive to startup and shutdown operation procedures. It is observed that, by implement the initial controller instead of the updated controller, fatigue damage of the transient processes during startup operations in above rated wind speed environmental conditions results in a considerable increase of the short-term fatigue damage, e.g. the short-term fatigue damage of the 5-MW-CSC in F610, F710, and F810 are increased by 18.6%, 42.4%, and 34.0%, respectively.

The long-term fatigue damage assessment, which is given in Section 5.5, indicates that, for both models, the nominal axial stresses in the tower base may need to be reduced by up to 50% to ensure sufficient safety margin for fatigue damage.

Within the reduction range, it is observed that the relative importance of fatigue damage due to the transient load processes significantly increase with decrease of the nominal axial stresses. The relative importance of fatigue damage can be represented by the relative differences between fatigue damage of a case with and without the transient load processes. We denote the percentage of the relative difference as R_d. Consequently, the increased relative importance can be seen by comparing corresponding R_d in Tables 6 and 7. For example, by reducing the nominal axial stresses of the transient and stationary processes by 50%, R_d of the 5-MW-CSC in F310 is tripled from 23% to 67%.

This is because the reduction of the nominal axial stresses in tower base makes more stress ranges to be lower than the stress range value which corresponds to the stress range at 10^7 cycles of the corresponding SN curves shown in Table 5. Consequently, fatigue damage of these cycles tend to be proportional to 5th order (m_2) rather than 3rd order (m_1) of the stress ranges and be more sensitive to fatigue damage induced by the cycles with large stress ranges in transient load processes.

This is supported by results of a parametric study shown in the plot with respect to α and the R_d in Figure 14. In the parametric study, fatigue damage rates induced by realizations of nominal axial stresses of point 3 and point 7 on the tower base and tower top of the 5-MW-CSC and OC4 Semi in the selected cases with and without the transient load processes, with and without application of $\eta_r = 0.5$, and with C1, D and F SN curves are calculated. We denote fatigue damage rate induced by a given realization in a given situation as d. Then, the R_d and α are calculated correspondingly. R_d is the percentage of the relative difference as mentioned above. α is defined as a ratio between number of the cycles which exceed the corresponding stress range at 10^7 cycles of corresponding SN curve and the total number of the cycles of the realization.

The results of the parametric study shown in Figures 14 and 15 also show that, in general, 2 degree/s shutdown operation results in more fatigue damage than 8 degree/s shutdown operation. This agrees with the analysis shown in Section 5.3.1.

Table 6 Short-term fatigue damage rates with respect to 4,600 seconds simulated axial stress of point 3 on tower base and SN curve C1 and updated controller. By using the updated controller, fatigue damage during each startup operation of both floating wind turbines in environmental conditions from F400 to F820 is reduced compared to the use of the initial controller

Fatigue damage rate	5-MW-CSC operational condition (without transient load processes)	5-MW-CSC operational condition with transient load processes induced by startup and shutdown (8 degrees/seconds)	Percentage of the change of damage due to the transient load effect R_d [%]	OC4 Semi operational condition (without transient load processes)	OC4 Semi operational condition with transient load processes induced by startup and shutdown (8 degrees/seconds)	Percentage of the change of damage due to the transient load effect R_d [%]
F100	$2.49 * 10^{-6}$	$3.45 * 10^{-6}$	39	$1.09 * 10^{-5}$	$9.02 * 10^{-6}$	-17
F110	$2.48 * 10^{-6}$	$3.34 * 10^{-6}$	34	$1.09 * 10^{-5}$	$8.66 * 10^{-6}$	-20
F120	$2.28 * 10^{-6}$	$3.00 * 10^{-6}$	32	$1.01 * 10^{-5}$	$8.67 * 10^{-6}$	-14
F200	$6.37 * 10^{-6}$	$8.10 * 10^{-6}$	27	$1.46 * 10^{-5}$	$1.39 * 10^{-5}$	-5
F210	$5.75 * 10^{-6}$	$7.44 * 10^{-6}$	30	$1.26 * 10^{-5}$	$1.23 * 10^{-5}$	-3
F220	$4.37 * 10^{-6}$	$5.91 * 10^{-6}$	35	$1.02 * 10^{-5}$	$9.55 * 10^{-6}$	-6
F300	$1.55 * 10^{-5}$	$1.85 * 10^{-5}$	20	$1.47 * 10^{-5}$	$1.69 * 10^{-5}$	14
F310	$1.06 * 10^{-5}$	$1.32 * 10^{-5}$	24	$9.08 * 10^{-6}$	$9.94 * 10^{-6}$	9
F320	$8.09 * 10^{-6}$	$1.10 * 10^{-6}$	36	$5.39 * 10^{-6}$	$6.52 * 10^{-6}$	21
F400	$3.73 * 10^{-5}$	$3.94 * 10^{-5}$	6	$3.31 * 10^{-5}$	$3.30 * 10^{-5}$	0
F410	$2.42 * 10^{-5}$	$2.50 * 10^{-5}$	3	$1.52 * 10^{-5}$	$1.57 * 10^{-5}$	3
F420	$1.79 * 10^{-5}$	$1.92 * 10^{-5}$	7	$6.74 * 10^{-6}$	$7.03 * 10^{-6}$	4
F500	$3.62 * 10^{-5}$	$3.65 * 10^{-5}$	1	$4.97 * 10^{-5}$	$4.94 * 10^{-5}$	-1
F510	$1.73 * 10^{-5}$	$1.86 * 10^{-5}$	8	$1.92 * 10^{-5}$	$1.87 * 10^{-5}$	-3
F600	$4.86 * 10^{-5}$	$4.81 * 10^{-5}$	-1	$8.50 * 10^{-5}$	$8.36 * 10^{-5}$	-2
F610	$1.69 * 10^{-5}$	$1.70 * 10^{-5}$	1	$2.85 * 10^{-5}$	$2.85 * 10^{-5}$	-2
F700	$6.11 * 10^{-5}$	$5.99 * 10^{-5}$	-2	$1.10 * 10^{-4}$	$1.08 * 10^{-4}$	-1
F710	$1.97 * 10^{-5}$	$2.01 * 10^{-5}$	2	$3.41 * 10^{-5}$	$3.34 * 10^{-5}$	-2
F720	$1.07 * 10^{-5}$	$1.15 * 10^{-5}$	8	$1.80 * 10^{-5}$	$1.82 * 10^{-5}$	1
F800	$7.19 * 10^{-5}$	$6.96 * 10^{-5}$	-3	$1.38 * 10^{-4}$	$1.34 * 10^{-4}$	-3
F810	$2.16 * 10^{-5}$	$2.19 * 10^{-5}$	1	$4.15 * 10^{-5}$	$3.92 * 10^{-5}$	-6
F820	$1.17 * 10^{-5}$	$1.34 * 10^{-5}$	14	$2.23 * 10^{-5}$	$2.17 * 10^{-5}$	-3

Table 7 Selected short-term fatigue damage rates with respect to 4,600 seconds simulated axial stress of point 3 on tower base with $\eta_r = 0.5$ and C1 SN curve. η_r is defined as a reduction factor. $\eta_r = 0.5$ means that the stresses have been reduced to 50% of the stress level corresponding to Table 6

Fatigue damage rate with $\eta_r = 0.5$	5-MW-CSC operational condition	5-MW-CSC operational condition with startup and shutdown (8 degrees/s)	Percentage of the change of damage due to the transient load effect R_d [%]	OC4 Semi operational condition	OC4 Semi operational condition with startup and shutdown (8 degrees/s)	Percentage of the change of damage due to the transient load effect R_d [%]
F110	$0.84 * 10^{-7}$	$2.03 * 10^{-7}$	142	$3.81 * 10^{-7}$	$3.60 * 10^{-7}$	-6
F210	$2.43 * 10^{-7}$	$4.73 * 10^{-7}$	95	$4.59 * 10^{-7}$	$5.40 * 10^{-7}$	18
F310	$0.61 * 10^{-6}$	$1.02 * 10^{-6}$	67	$3.87 * 10^{-7}$	$5.95 * 10^{-7}$	54

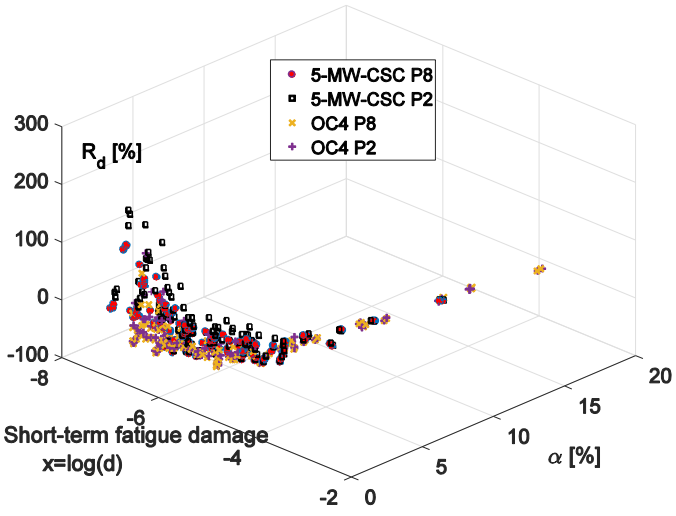

(a) 3D plot

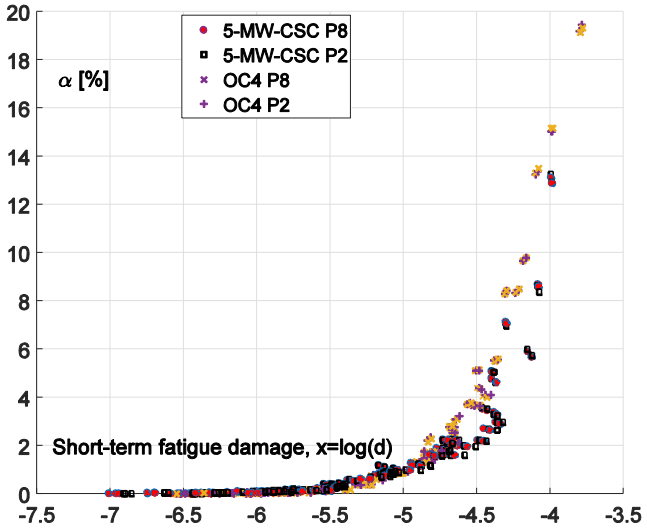

(b) Top view (X-Y view)

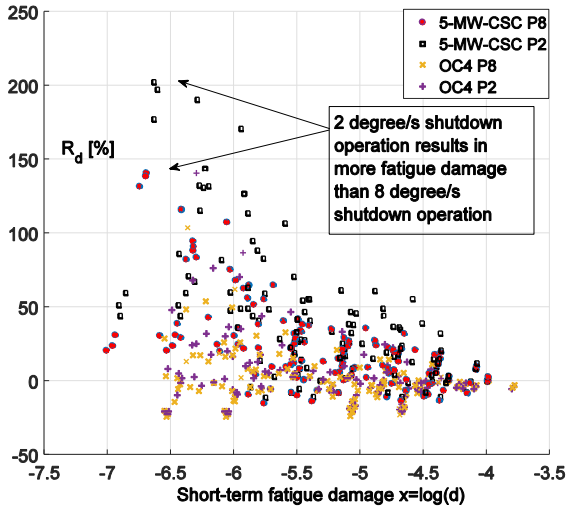

(c) Side view 1 (X-Z view)

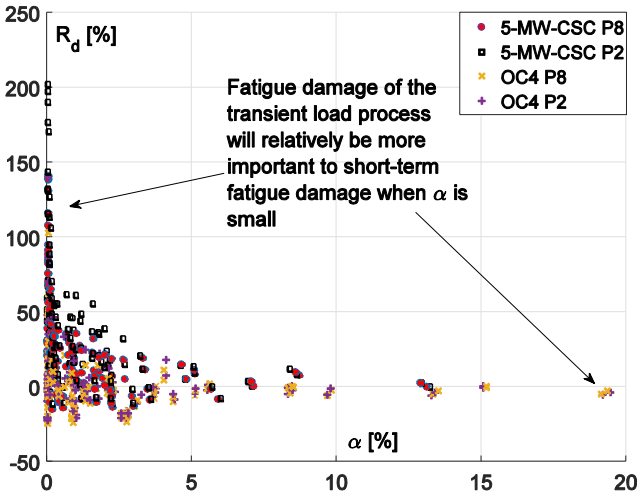

(d) Side view 2 (Y-Z view)

Figure 14 Plot of (d, α, R_d) of each simulated nominal axial stress realization on tower base. R_d for the 5-MW-CSC P8 means relative difference between fatigue damage rates of the 5-MW-CSC with and without 8 degrees/s control for pitch angles of the blades. For a result point of 5-MW-CSC P8, d of the result point is the fatigue damage rate of the 5-MW-CSC with 8 degrees/s pitch blade control in the corresponding short-term environmental condition. α is the ratio corresponds to the short-term fatigue analysis for which α is defined as a ratio between number of the stress cycles which exceed the corresponding stress range at 10^7 cycles and the total number of the stress cycles identified from the short-term fatigue analysis

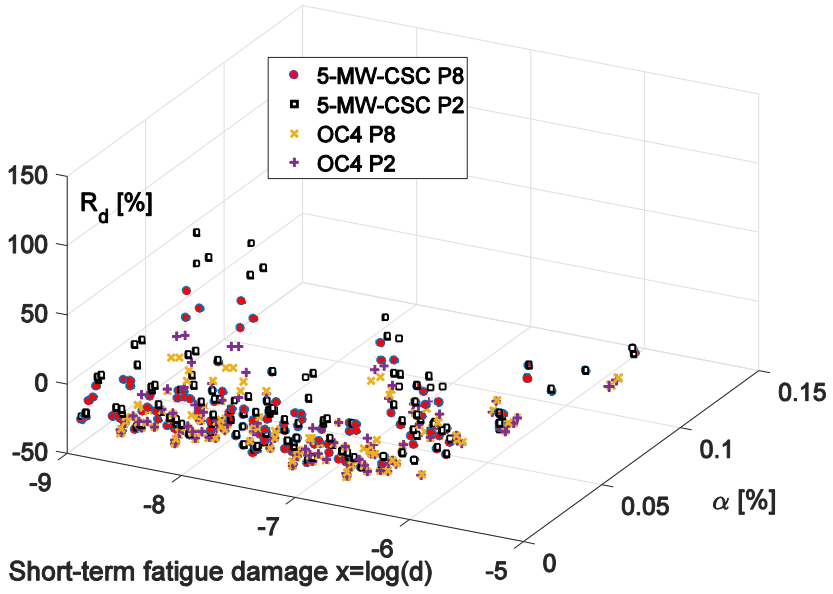

Figure 15 Plot of (d, α, R_d) of each simulated nominal axial stress realization on tower top.

5.5 Importance of the transient load processes on the long-term fatigue damage

The effect of the startup and shutdown induced transient load process on long-term fatigue damage is related to R_d, fatigue damage rate of each short-term environmental condition, duration between startup and shutdown, and occurrence probability of the corresponding environmental condition.

As far as the authors know, by now, publically accessible information with respect to average duration between startup and shutdown is very limited. As tabulated in Table 1, the average duration between two consecutive shutdown events due to fault state or maintenance (Shutdown Event Group A) of the analyzed land-based wind turbines by Valerie et al (2013) is 39 hours. While, occurrence probability of Shutdown Event Group B, for which shutdown events initiated by the control system of the wind turbine as measurements exceed alarm limiting values specified by operators but are below the limiting values for activating the safety system of the wind turbine, is expected to be higher than Shutdown Event Group A.

We assume that averaged duration between a startup and shutdown is n hours. As a result, by accounting for fatigue damage due to the operation, long-term fatigue damage (denoted as D_{total,tra_inc}) can be expressed by Eq. (6). N^{20yr} is the total amount of hours in 20 years. d_i and $d_i(1+R_{d,i})$ represent corresponding expected 1-hour short-term fatigue damage with and without fatigue damage of transient load processes induced by corresponding startup-shutdown operation. $R_{d,i}$ is the corresponding relative difference.

$$D_{total,tra\_inc} = N^{20yr}\sum_{i=1}^{N^{lc}} d_i p_i (1+\frac{R_{d,i}}{n}) \qquad (6)$$

Results of the parametric study presented in Section 5.4 show $R_{d,i}$ of 5-MW-CSC could fall in range from -15% to 205%. As shown in Section 5.4, the parametric study is with respect to different reduction level of the nominal axial stresses and different SN curves.

To conservatively estimate the effect of startup and shutdown processes, $R_{d,i}$ in Eq. (6) could be replaced by its upper range, i.e. 205%. Consequently, it can be easily derived that relative increase of long-term fatigue damage induced by fatigue damage of the transient load processes is $\frac{205\%}{n}$. If n is 39, this means the increased fatigue damage rate is no more than 5.3% and is not important when compared to uncertainties in fatigue damage rate assessment. While, if n is 8, it means that the fatigue damage rate may be increased by 25%. This may need to be kept in mind.

The range of the of the reduction level in the parametric study is identified on base of a very rough estimate with respect to total fatigue damage of the 5-MW-CSC operating in operational stationary processes in 20 years. When fatigue damage is calculated by using the SN curve C1, the total fatigue damage of the tower base of the 5-MW-CSC is $20*365*24*\frac{3,600}{4,600}*1.21*10^{-5}=1.66$,

which is larger than 1 while the corresponding fatigue damage of the OC4-Semi is even larger. $1.21 * 10^{-5}$ is the averaged 4,600 seconds fatigue damage rate and is obtained by summing corresponding product of each short-term fatigue damage rate of the 5-MW-CSC given in Table 6 and its corresponding occurrence probability given in Table 3.

The results of the rough estimate indicate that the nominal axial stresses in the tower base need to be reduced to increase the safety margin for fatigue damage. Possible approaches could be 1) to increase thickness of the tower; and 2) to optimize the control system to increase aerodynamic damping stationary operational processes.

For the 5-MW-CSC, it is not likely that the nominal axial stresses have to be reduced by more than 50%. This is because that, in the most critical situation for which fatigue damage is calculated by using SN curve F, the 50% reduction makes the estimated total fatigue damage be reduced to 0.7 which means sufficient safety margin for fatigue damage.

It should be emphasized that estimates with respect to the total fatigue damage is based on only 22 environmental conditions. Uncertainties in the estimates should be kept in mind.

5 CONCLUSIONS

Short-term fatigue damage rates in twenty two environmental conditions with and without transient load processes induced by startup and shutdown of the wind turbines are compared to shed light on importance of the transient load processes on the fatigue damage on the tower top and tower base of two semi-submersible wind turbines.

Responses of the semi-submersible wind turbines are simulated by a state-of-the-art time-domain computer code for which the control system for startup and shutdown operations and flexibility of the blades and tower have been appropriately modelled.

Fatigue damage of the tower base and tower top is dominated by the cyclic variation of the fore-aft bending moments, while fatigue damage induced by variations of shear stresses is negligible. Transient load processes induced by startup and shutdown may result in the cycles with relatively large stress ranges compared with the cycles induced by wind and wave loads in a stationary operational condition and result in larger fatigue damage rate.

It is challenging to startup semi-submersible wind turbines in the above rated wind condition since blade pitch angles need to be well adjusted in accordance to the rotor rotational speed to reduce aerodynamic loads on the rotor during the process that the rotor is speeded up to its rated rotational speed. Based on the NREL-developed controller, an updated controller is established and used to significantly mitigate the transient load processes during startup operation in above rated winds comparing to the initial controller. Therefore, the updated controller rather than the initial controller is used in simulations analyzed in the present paper.

The simulated results show that extreme aerodynamic load on floating wind turbine rotors during shutdown operation might be reduced by slowing down pitch rotational speed of the blades; however at the expense more fatigue damage. This is due to the fact that hydrodynamic and aerodynamic load effects which are coupled with the blade pitch angle control and dynamic motions of the model. Due to the same fact, simulation results show a fatigue damage rate for the 5-MW-CSC could be more sensitive to the transient load process than the OC4 Semi.

For the 5-MW-CSC, the transient load processes due to shutdown operation can result in considerable increase of short-term fatigue damage for the tower base and tower top in below and at rated wind speed conditions with an occurrence probability more than 70%.

The calculated fatigue damage rate indicates that the nominal axial stresses in the tower base of both floating wind turbines need to be reduced to ensure sufficient safety margin for fatigue damage in accordance to corresponding design standards. The reduction makes more cycles with stress ranges below the stress range at 10^7 cycles of corresponding SN curve. Within a reasonable reduction range, i.e. no more than 50%, the relative importance of fatigue damage due to the transient load processes significantly increase with a decrease of the nominal stress level.

A parametric study with respect to different SN curves and reduction percentages for the nominal axial stresses shows that, for the 5-MW-CSC, relative differences between short-term fatigue damages for tower base and tower top with and without the transient load processes could fall in range from -15% to 205% based on a modified NREL controller. The relative differences may be reduced by developing and implementing an even more advanced control system; however cost of increasing of complexity and reduction of reliability of the control system should also be considered.

The effect of the transient load process induced by start-ups and shut-downs on the long-term fatigue damage is related to the average time between startup and shutdown. For the tower base of the 5-MW-CSC, the transient load process could be important to consider for the long-term fatigue damage design if the time between startup and shutdown events is relative short, e.g. 8 hours. A reliability study (Valerie et al 2013) based on measurements of land based wind turbines show that the average time between events involving a fault state or maintenance (known as “Shutdown Event Group A”) is 39 hours. In addition to Shutdown Event Group A, many shutdown events occur when measurements exceed alarm limiting values specified by operators but are below to the limiting values for activating the safety system of the wind turbine (known as “Shutdown Event Group B”) exist in real. The occurrence probability of Shutdown Event Group B is expected to be higher than Shutdown Event Group A. More publication with respect to data for Shutdown Event Group B is recommended since, by now, relevant publicly accessible data is very limited

ACKNOWLEDGMENTS

The authors acknowledge the grant from Equinor ASA (formerly Statoil) and financial support provided by the Research Council of Norway through the Centre for Ships and Ocean Structures; the Norwegian Research Centre for Offshore Wind Technology (NOWITECH), NTNU; and the Centre for Autonomous Marine Operations and Systems (AMOS), NTNU..

REFERENCES

ABS, (2013), "Guide for Building and Classing Floating Offshore Wind Turbine Installations", American Bureau of Shipping.

Bachynski, E.E., Etemaddar, M., Kvittem, M.I., Luan, C., Moan, T., (2013) "Dynamic analysis of floating wind turbines during pitch actuator fault, grid loss, and shutdown", Energy Procedia vol. 35, 210-222. doi:10.1016/j.egypro.2013.07.174

Bachynski, E.E., (2014). "Design and Dynamic Analysis of Tension Leg Platform Wind Turbines", Ph.D thesis, Norwegian University of Science and Technology, Trondheim, Norway

Brodtkorb, P.A., Johannesson, P., Lindgren, G., Rychlik, I., Ryd én, J. and S ö, E. (2000). "WAFO - a Matlab toolbox for analysis of random waves and loads", Proc. 10th Int. Offshore and Polar Eng. Conf., Seattle, USA, Vol III, pp. 343-350.

Burton, T., Jenkins, N., Sharpe, D. and Bossanyi, E., (2011), "*Wind energy handbook*", John Wiley & Sons.

Butterfield, S., Musial, W., Jonkman, J. and Sclavounos, P., (2007), "Engineering challenges for floating offshore wind turbines", Technical report NREL/CP-500-38776, National Renewable Energy Laboratory

ClassNK, (2012), "Guidelines for Offshore Floating Wind Turbine Structures", Nippon Kaiji Kyokai.

DNV, (2010a), "Recommended Practice – Fatigue Design of Offshore Steel Structures", DNV-RP-C203, Det Norske Veritas.

DNV, (2010b), "Recommended Practice - Environmental Conditions and Environmental Loads", DNV-RP-C205, Det Norske Veritas.

DNV, (2011), "Design of Offshore Steel Structures, General (LRFD Method)", DNV-OS-C101, Det Norske Veritas.

DNV, (2013), "Offshore standard – Design of Floating Wind turbine Structures", DNV-OS-J103, Det Norske Veritas.

DNVGL, (2012), "Certification of Offshore Wind Turbines Guideline – Edition 2012".

Faltinsen, O.M., (1990), "Sea loads on ships and offshore structures", Cambridge University Press, UK.

IEC, (2005), "Wind turbines – Part 1: Design requirements", IEC-61400-1, International Electrotechnical Commission.

IEC, (2009), "Wind turbines: Part 3: Design requirements for offshore wind turbines", IEC-61400-3, International Electrotechnical Commission.

Jiang, Z., Moan, T., Gao, Z., and Karimirad, M., (2013), "Effect of Shut-Down Procedures on the Dynamic Responses of a Spar-Type Floating Wind Turbine", 32nd International Conference on Ocean, Offshore and Arctic Engineering, OMAE2013-10214, Nantes, France, June 9–14.

Jonkman, B.J., (2009), "TurbSim User's Guide: Version 1.50" ", NREL/TP-500-46198, National Renewable Energy Laboratory, Golden, CO, U.S.A.

Jonkman J., Butterfield, S., Musial, W. and Scott, G., (2009), "Definition of a 5-MW Reference Wind Turbine for Offshore System Development", NREL/TP-500-38060, National Renewable Energy Laboratory, Golden, CO, U.S.A.

Jonkman J., (2010), "Definition of the Floating System for Phase IV of OC3", NREL/TP-500-47535, National Renewable Energy Laboratory, Golden, CO, USA

Kvittem, M. I., Moan, T., (2015), "Time domain analysis procedures for fatigue assessment of a semi-submersible wind turbine", Marine Structures. vol. 40, pages 38-59, https://doi.org/10.1016/j.marstruc.2014.10.009.

Larsen, G. and Thomsen, K., (1996), "A Simple Approximative Procedure for Talking into Account Low Cycle Fatigue Loads," Proc. IEA 4th Symposium of Wind Turbine Fatigue, IEA.

Li, L., Gao, Z., Moan, T., (2015), "Joint Distribution of Environmental Condition at Five European Offshore Sites for Design of Combined Wind and Wave Energy Devices", Journal of Offshore Mechanics and Arctic Engineering. 137(3), 031901 (16 pages). doi: 10.1115/1.4029842.

Lotsberg, I., (2016), "Fatigue design of marine structures", Cambridge University Press, UK.

Luan, C., Gao, Z., and Moan, T., (2016), "Design and analysis of a braceless steel 5-mw semi-submersible wind turbine", In 35th International Conference on Ocean, Offshore and Arctic Engineering, OMAE2016-54848, Busan, Korea, June 19–24.

Luan, C., Gao, Z., and Moan, T., (2017), "Development and verification of a time-domain approach for determining forces and moments in structural components of floaters with an application to floating wind turbines", Marine Structures, Volume 51, pages 87-109, https://doi.org/10.1016/j.marstruc.2016.10.002.

Luxcey, N., Ormberg, H., and Passano, E., (2011), "Global analysis of a floating wind turbine using an aero-hydro-elastic numerical model. Part 2: Benchmark study". In 30th International Conference on Ocean, Offshore, and Arctic Engineering,no, OMAE2011-50088, Rotterdam, Netherlands.

MARINTEK, (2011). SIMO User's Manual.

MARINTEK, (2013). RIFLEX User's Manual.

Marsh G., Wignall, C., Thies, P., Barltrop, N., Incecik, A., Venugopal, V., and Johanning, L., (2016), "Review and application of Rainflow residue processing techniques for accurate fatigue damage estimation", International Journal of Fatigue.

Moan, T., (2015), “Recent development of analysis and design of offshore wind turbines for deep water”. Renewable Energies Offshore - 1st International Conference on Renewable Energies Offshore, RENEW 2014, Lisbon, Portugal.
Moan, T., Gao, Z., Bachynski, E., and Nejad, A., (2020), “Recent Advances in Integrated Response Analysis of Floating Wind Turbines in a Reliability Perspective”, Journal of OMAE.
Moriarty, P. J., and Hansen, A. C., (2005), AeroDyn theory manual, Tech. Rep, NREL/TP-500-36881.
Mouzakis, F., and E. Morfiadakis, (1997), “Identification of Low Cycle Effects on Wind Turbine
Component Lifetime Estimation,” BWEA ’97.
Nejad, A.R., Bachynski, E.E., Kvittem, M.I., Luan, C., Gao, Z. and Moan, T., (2015), “Stochastic Dynamic Load Effect and Fatigue Damage Analysis of Drivetrains in Land-based and TLP, Spar and Semi-Submersible Floating Wind Turbines”, Marine Structures, Vol 42, pp 137–153.
Ormberg, H., Passano, E., and Luxcey, N., (2011), “Global analysis of a floating wind turbine using an aero-hydro-elastic model. Part 1: Code development and case study”. In 30th International Conference on Ocean, Offshore, and Arctic Engineering,no, OMAE2011-50114, Rotterdam, Netherlands.
Ormberg, H., and Bachynski, E. E., (2012). “Global analysis of floating wind turbines: Code development, model sensitivity and benchmark study”. In 22nd International Ocean and Polar Engineering Conference, Vol. 1, pp. 366–373.
Robertson, A., Jonkman, J., Masciola, M., Song, H., Goupee, A., Coulling, A., and Luan C., (2012), “Definition of the Semisubmersible Floating System for Phase II of OC4”, Offshore Code Comparison Collaboration Continuation (OC4) for IEA Task 30.
Van der Hoven, I., (1957), “Power spectrum of horizontal wind speed in the frequency range from 0.0007 to 900 cycles per hour”, Journal of Meteorology, 14(2):160–164.
Sutherland, H.J., (1999), “On the fatigue analysis of wind turbines”, Sandia National Laboratories, New Mexico 87185-0708.
Valerie et al, (2012), “Continuous Reliability Enhancement for Wind (CREW) Database> Wind Plant Reliability Benchmark”.
Valerie et al, (2013), “Continuous Reliability Enhancement for Wind (CREW) Database> Wind Plant Reliability Benchmark”.